Optics Communications 322 (2014) 227–233

Contents lists available at ScienceDirect

Optics Communications

journal homepage: www.elsevier.com/locate/optcom

Ultra-broadband and ultra-low-loss photonic crystal with band-flatness waveguide 60° bend obtained based on lattice-shifted optimization

Jian Zhou [a], Huiping Tian [a], Daquan Yang [a,b], Yuanyuan Liu [c], Qi Liu [a], Yuefeng Ji [a,*]

[a] The State Key Laboratory of Information Photonics and Optical Communications, School of Information and Communication Engineering, Beijing University of Posts and Telecommunications, Beijing 100876, China
[b] School of Engineering and Applied Sciences, Harvard University, Cambridge, MA 02138, USA
[c] Institute of Semiconductors, Chinese Academy of Science, Engineering Research Center for Semiconductor Integrated Technology, Beijing, China

ARTICLE INFO

Article history:
Received 6 December 2013
Received in revised form
4 February 2014
Accepted 4 February 2014
Available online 26 February 2014

Keywords:
Photonic crystal slab
Silicon-on-insulator (SOI)
Broadband
Low loss
Waveguide bend

ABSTRACT

This work discusses a novel design for a W1 (one missing row of holes) waveguide 60° bend implemented based on photonic crystal slab in a silicon-on-insulator (SOI) material. The bend has been designed to exhibit broadband and low loss for single-mode operation. The investigated design improvement depends on displacing holes in the bending region, meanwhile adjusting the size of air holes to achieve low dispersion and the transmission spectrum presents flatness over 180 nm bandwidth around 1550 nm. By means of rigorous three-dimensional finite-difference time-domain (3D-FDTD) technique, the 3-dB bandwidth reaches 216 nm and we demonstrate a ultralow-loss output of optimized bend waveguide with an average loss of 0.71 ± 0.19 dB in the broadband range 1462–1643 nm, which covers the entire C-band of optical communication.

1. Introduction

Yablonovitch [1] and John [2] suggested the possibility to confine the propagation of photons with energy located within certain bands by creating an artificial periodicity in dielectric materials. Such structures are often regarded as photonic crystals (PhCs) and have drawn a lot of attention due to its unique photonic band gap (PBG). As a novel type of light guiding device, PhC waveguides have the advantages of low loss and compactness, and they have become a promising candidate to be a key component in Photonic Integrated Circuits (PICs) [3–6]. In recent years, planar PhC devices are often referred as triangular arrangements of low dielectric pillars in a high dielectric material, and they are relatively easy to fabricate with conventional semiconductor processing technology, which have been the object of extensive research [7–9]. Planar PhCs based on above configuration provides a large PBG for the transverse-electric (TE) polarization [10]. Defects in the PhC can introduce guided modes in the PBG. Due to the triangular lattice structure, such PhCWs are naturally bent in steps of 60°, consequently, making the 60° PhCW bend a critical component in PhC-based PICs.

The waveguide bend is among the most basic integrated-optics building blocks. Compared with straight PhC waveguide, when the lightwave encounters a waveguide bend, it usually suffers great loss because of the large bending angle. The bandwidth of high transmission will also be limited to a narrow range. Beyond that the transmission spectrum usually presents large fluctuation on broadband. In order to reduce the bending loss, increase the bandwidth and relieve the spectrum fluctuation, large amount of efforts have been made to improve the performance of waveguide bends, including adjusting the positions of air holes [11,12], changing the radius of certain air holes at the bend corner [13,14], smoothing the bend and changing the local width of the waveguide [15], adding some air holes into the bend path [16], selective optofluidic infiltration of an air hole [17]. Besides, Si-based type-B antiresonant reflecting optical waveguide (ARROW-B) photonic crystal waveguides (PhCWs) [18] and topology optimization [19,20] are also another methods used in bend structure design. However, the design drawback of these structures is that they cannot typically operate with broadband and low loss at the same time. Examples of such systems include that of Bakhshi et al. [17] who demonstrated a procedure to enhance the transmission efficiency of 60° photonic crystal waveguide bends by means of selective optofluidic infiltration of an air hole and Ren

* Corresponding author at: P.O. Box 90, No. 10, Xi Tu Cheng Road, Beijing 100876, China.
E-mail addresses: hptian@bupt.edu.cn (H. Tian), jyf@bupt.edu.cn (Y. Ji).

http://dx.doi.org/10.1016/j.optcom.2014.02.018
0030-4018

et al. [14] who demonstrated a simply modified bend structure based on guided modes mechanism. The bandwidth of above two structures is only 88 nm and 116 nm with transmission over 90%, respectively. Chen et al. [18] demonstrated Si-based type-B anti-resonant reflecting optical waveguide (ARROW-B) photonic crystal waveguides but the minimum bend loss of 60° photonic crystal bend waveguide reached 4.2 dB/bend within the range of bandwidth. In addition, as mentioned above, the transmission spectrum appears flat band only in the range of narrow bandwidth.

To obtain high bandwidth, low loss, and broadband flatness of the waveguide bends, this work discusses the optimization of a 60° bend in the W1 waveguide in the substrate-type Silicon-on-insulator (SOI) material system. For the triangular lattice, 60° bends are obtained from the lattice symmetry but are normally submitted to light reflection due to mode conversion and modal mismatch in the bending region. We propose a single-mode W1 waveguide bend optimized that combines varying hole sizes in the bending region with the local displacement of individual holes. Although extensive researches have been made above the optimization of PhC waveguides bends, in terms of our best knowledge no systematic study of 60° bends depending on uniform hole size for simplified process control has been presented to date. With a three dimensional finite-difference time-domain (3D-FDTD) technique, the 3-dB bandwidth reaches 216 nm whilst we demonstrate an ultra-low loss (in the range 0.71 ± 0.19 dB, transmission efficiency over 90%) in the broadband range 1462–1643 nm. In addition, the transmission spectrum presents flat band over 180 nm bandwidth around 1550 nm. More importantly, we only consider mainly shifting two independent holes and slightly modifying the sizes of holes surrounding the corner, from a practical point of view, which will make the designs relatively simple for further fabrication.

2. Design and analysis of conventional 60° waveguide bend

Silicon-on-insulator (SOI) is an excellent choice of material for a monolithic integration PhC-based PICs and optical devices. We define the PhC structures in the top silicon layer of a SOI material. Fig. 1 shows 3D schematic diagram of our 60° waveguide bend structure using SOI substrate. In addition, the specified PhCs are defined as air holes arranged in a triangular lattice and the PhCWs are carved out as W1 waveguides by removing one row of holes in the nearest-neighbor direction of the crystal lattice. This is because that compared with square lattice PhC, a triangular lattice can be a great advantage to acquire a wider PBG. With regard to the pillar-array PhC, hole-array with a strong refractive-index contrast is easier to form a suspended free-standing membrane. Based on this system, the defect mode may lie partly below the cladding light line in the k–ω plane [21]. In this case the mode is truly guided with no intrinsic diffraction loss (unlike modes above the light line which are subject to intrinsic out-of-plane losses). Therefore in order to obtain larger PBG and small vertical loss, the structure design in this work is based on the triangular lattice, hole-array based PhC (Fig. 1). In our paper, plane wave expansion (PWE) method and the open source FDTD software Meep are used to calculate their photonic band structure and transmission spectra, respectively [22]. We set the light source at the head of the input W1 waveguide and monitor was located at the end of the output W1 waveguide. In our simulations, we use the TE polarized Gaussian-pulse source (pulse light source centered at $\lambda = 1.55$ um) as the incident source. The simulations are performed by using Meep to observe the steady state electric field and the transmission spectra. For improving accuracy in the simulation, FDTD analysis of photonic crystal structure is carried out with a mesh size of $a/20$ and time step of $0.025a/c$, where a is the lattice

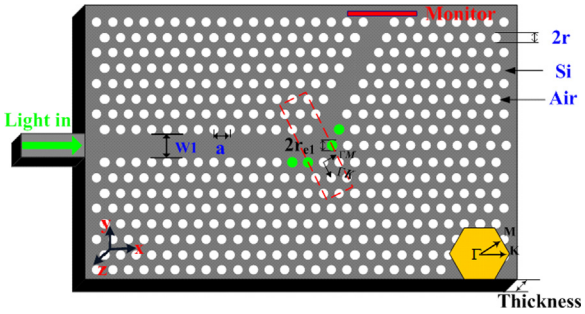

Fig. 1. Schematic representation of the conventional 3D 60° PhC waveguide bends, where $a=385$ nm, $r=0.32a=123.2$ nm, $T=0.578a=222.53$ nm. The rectangle of dimensions $2a \times 6a$, depicted by the red dashed lines, represents the real-space supercell for the bend. (For interpretation of the references to color in this figure legend, the reader is referred to the web version of this article.)

constant. All the simulations are carried out with the same mesh size and time step for future comparable results. Since the boundary conditions at the spatial edges of the computational domain must be carefully considered. The simulation area in our paper is surrounded by one-spatial unit thick perfectly matched layer (PML), in which both electric and magnetic conductivities are introduced in such a way that the wave impedance remains constant, absorbing the energy without inducing reflections.

As shown in Fig. 1, the PhCW bend is modeled by a planer PhC with a triangular lattice PhC of air holes. The PhC structure has a pitch of $a=385$ nm in a triangular configuration of air holes of diameter $d=246.4$ nm. The slab thickness is that $T=0.578$ $a=222.53$ nm realized on silicon slab waveguide. The rectangle of dimensions $2a \times 6a$, depicted by the red dashed lines, represents the real-space supercell by which one can obtain the reduced Brillouin zone for the 60° PhCW bend. It has already been demonstrated that for this choice of parameters, within the experimental fabrication tolerances, the numerical results for major transmission features including transmission levels obtained by 3D simulations correctly predict the measured data in the 1550 nm wavelength range [23]. We focus on the transmission levels centered about $\lambda_0=1550$ nm or the normalized frequency of $a/\lambda_0=0.2408$. Using the plane wave expansion (PWE) method, the normalized PBG for the TE polarization is calculated to be in the range of $0.2217 \le a/\lambda \le 0.3156$. The straight waveguide is along the Γ–K direction. At the corner of the bend, there are three rows of airholes along the symmetric axis of the bend. This corner can be considered as a short waveguide along the Γ–M direction, and the guided mode in it is considered to be transient guided mode [24]. Directions Γ–K and Γ–M are labeled on the figure showing the directions along which the light propagates with propagation constants $k_{\Gamma K}$ and $k_{\Gamma M}$, respectively.

According to the description in [25], in order to improve the PhC bend transmission efficiency, we should reduce the reflection loss. Owing to the nature of PBGs, unlike conventional waveguides, PhCW do not experience radiation loss. As depicted in [26], the reflection coefficient of the waveguide bend can be expressed as

$$R(\omega) = \left[1 + \left(\frac{2k_{\Gamma K}(\omega)k_{\Gamma M}(\omega)}{(k_{\Gamma K}^2(\omega) - k_{\Gamma M}^2(\omega))\sin(k_{\Gamma M}(\omega)L)}\right)\right]^{-1} \quad (1)$$

where $k_{\Gamma K}$ and $k_{\Gamma M}$ are the wave numbers of the modes in the straight waveguide and the waveguide bend, respectively, and L is the equivalent length of the bend.

Using the plane wave expansion (PWE) method, we calculated the band structures of the waveguide along the Γ–K and Γ–M direction as shown in Fig. 2. In Fig. 2(a) and (b), the horizontal dashed lines indicate the normalized center frequency $a/\lambda_0=0.2408$. The guided modes of the straight waveguide and the bend waveguide are single

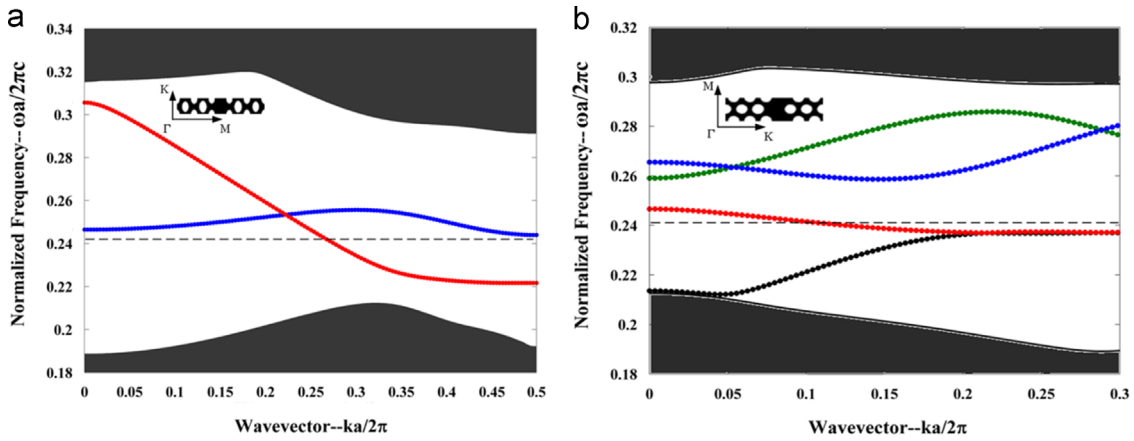

Fig. 2. Photonic band diagrams of light propagation in (a) ΓK direction and (b) ΓM direction. The black horizontal dashed lines indicate the normalized center frequency of $a/\lambda_0=0.2408$.

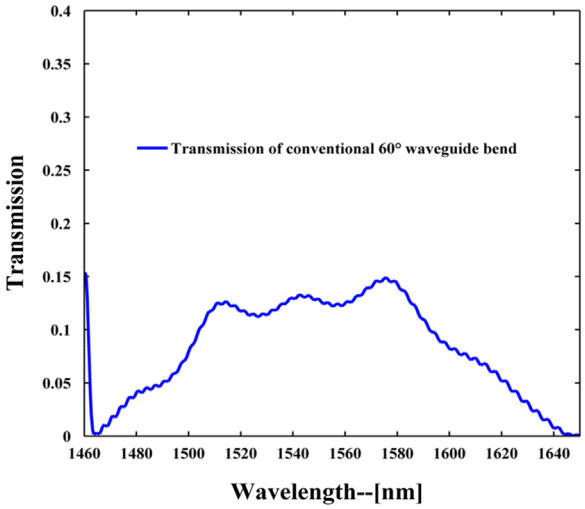

Fig. 3. Transmission spectrum for the conventional 60° PhC waveguide bends of Fig. 1.

mode based on the same frequency. The wavenumbers corresponding to this frequency equals to $0.2743(2\pi/a)$ and $0.1285(2\pi/a)$, respectively. We can easily examine that the band is folded once for the wavenumbers in the Γ–K direction, while the band is folded twice in the Γ–M direction. For the conventional triangular-lattice W1 waveguide in the Brillouin zone, the band diagram repeats with a period of $0.5(2\pi/a)$, and the corresponding $k_{\Gamma K}=(2\times0.5-0.2743)\times(2\pi/a)=0.7257(2\pi/a)$. Meanwhile, the band diagram folds with a period of $(2\times\sqrt{3})^{-1}\times(2\pi/a)=0.2888(2\pi/a)$ in the Γ–M direction, and the relevant $k_{\Gamma M}=(3\times0.2888-0.1285)\times(2\pi/a)=0.7379(2\pi/a)$. Finally, we can calculate $\Delta k=|k_{\Gamma K}-k_{\Gamma M}|=0.0122\times(2\pi/a)=2.594\times10^{-4}\,\mathrm{nm}^{-1}$. As can be seen from the expression (1), if the wavenumbers of the two modes (Δk) are closer ($\Delta k\to0$), the reflection will be smaller.

3. Optimization procedure of high-performance 60° bend waveguide

The transmission spectrum of the conventional bend waveguide calculated by the 3D-FDTD method is shown in Fig. 3. The transmission region ranges from $0.2379(2\pi c/a)$ to $0.2904(2\pi c/a)$ when the lattice constant $a=385$ nm. However the 3-dB bandwidth is small and the highest transmission efficiency is only about 0.15 at $0.2408(2\pi c/a)$. The main reason for low transmission is that the discontinuity at the bend region stimulates higher order modes that are evanescent in the photonic crystal waveguide. It should be mentioned that in the frequency range of 0.2379–$0.2904(2\pi c/a)$ the fundamental waveguide mode is below the light line and it cannot be coupled to the cladding mode. Therefore, the transmission is not affected by leakage of the fundamental mode to the cladding. The transmission spectra are obtained by integrating the poynting vector **S**, over a surface A, normal to the waveguide path [27]:

$$\mathbf{S}(r,\omega)=\frac{1}{2}E(r,\omega)\times H^{*}(r,\omega). \tag{2}$$

$$P=Re\left(\int_A \mathbf{S}(r,\omega)dA\right). \tag{3}$$

where E and H is the Fourier transforms of the electric and magnetic field components, respectively. As pointed out before, we use 3D-FDTD method to extract all field components (E_x, E_y and H_z), at the output ports of the bend. The photonic crystal bend consists of three parts: two waveguides in the Γ–K direction, each having two guided modes and one waveguides in the Γ–M direction, having one guided mode. In addition, in the conventional bend structure, the coupling of energy between these parts is not efficient and therefore the transmission of the bend is low. Based on the above theory analysis, to obtain high transmission is to match both the modes that their wave numbers of the straight waveguide and the waveguide bend.

In order to improve the transmission efficiency and bandwidth, we start the optimization subject by enlarging the four holes and indicated by green solid spheres in Fig. 1. This modification results in shifting the waveguide modes at the Γ–M direction upward in the diagram (Fig. 4) and hence brings about a better coupling of energy between the Γ–M and Γ–K direction waveguides. As a result, the bandwidth and spectrum are increased. Fig. 4 shows the transmission spectra for various radii of the introduced holes r_{e1}. Table 1 presents the computed 3-dB bandwidth for different values of r_{e1} and transmittance at $\lambda=1550$ nm. Fig. 5 directly demonstrates 3-dB bandwidth of the bend structure and transmittance at $\lambda=1550$ nm as a function of the air hole radius r_{e1}. As seen in Fig. 5, the air hole radius $r_{e1}=0.39a$ leads to showing a better result relative to other situations. The optimal transmission efficiency is only 0.254 while the 3-dB bandwidth reveals 115 nm. However, through changing the air hole radius, the transmission region ranges from $0.2387(2\pi c/a)$ to $0.2981(2\pi c/a)$ when $r_{e1}=0.39a$. Compared with conventional bend structure, the optimized transmission region improves by 21.2%. Based on the expression (1), the calculated $k_{\Gamma K}$ keeps constant, the varied hole

radius produces different $k_{\Gamma M}$, thus, the calculated $\Delta k = |k_{\Gamma K} - k_{\Gamma M}|$ appears different value. Furthermore, the different value of transmittance is obtained for changed hole radius. From Figs. 4 and 5, we can see that the simulation results agree well with the theoretical analysis.

Technological constraints have to be followed for an optimized structure design so as to further enlarge the bandwidth and transmission efficiency. To keep a good process latitude, we impose the following conditions on the optimization: (a) The shape of the holes shall remain unchanged; (b) holes may not overlap to avoid mask breakdown due to faceting [28]; (c) the lattice constant must be kept fixed except in the bending region; and (d) the bend must be symmetric in order to preserve reciprocity with respect to power transmission, meaning that the bending loss due to out-of-plane scattering should be independent of the propagation direction. The coupling of even and odd modes in the multi-mode region cannot be prevented by design, as the 60° bend structure always breaks the transversal symmetry of the waveguide. Since the single-mode frequency range is larger than multi-mode, it is more suitable for broadband power transmission. Therefore the optimization goal is to move the operating point into the frequency range.

As shown by means of a sensitivity analysis performed in [29], the holes that most strongly influence the transmission are the two holes at the apex of the bend (blue and red holes in Fig. 6). We therefore restrict ourselves to a rigorous optimization of these two holes to limit computational cost. The proposal for symmetry and the restriction to only the two holes closest to the apex of the bend leaves two optimization degrees of freedom: moving these two holes along the symmetry axis of the bend (black line in Fig. 6). The step size for the optimization of S was selected to be $0.01a$, corresponding to a hole position variation step of 5 nm for $a=429$ nm lattice constant. Although this value is not a good trade-off between accuracy and calculation time, the $\Delta\mathbf{S}$ (slight variable) has a great effect on flatness for transmission spectra (Fig. 7(a)). When $\Delta\mathbf{S}=0.33a$, the transmission spectrum appears strongly distorted due to the decrease in local effective index experienced the coming wave. And by adjusting r_{e2} and r_{e3} (Fig. 7 (b) and (c)), we have a wider frequency region where the wave number of the mode in the bend waveguide matches with that of the straight waveguide as shown in Ref. [30]. Fig. 7(a) shows that the transmission efficiency presents a great improvement with respect to the Fig. 4. Simultaneously, Fig. 7(b) and (c) reveal the transmission spectra versus the air hole radius r_{e2} and r_{e3}, respectively. Finally, Fig. 7(c) presents a flat, high-transmission, and broadband transmission spectrum.

We analyze the properties of the transmission spectra concerning the optimized 60° bend waveguide by changing the position and size of the air holes near the bend corner. Tables 2a–c display the computation of Bandwidth, T_{max}, T_{min}, and ΔT ($T_{max}-T_{min}$) (grey region in Fig. 7(a)–(c)) (Bandwidth is the 3-dB bandwidth of bend structure shown in Fig. 7(a)–(c).), respectively. The grey-region parameters ($\boldsymbol{T}_{max}$, T_{min}, and ΔT) are critical for the study of dispersion, and smaller ΔT indicates lower dispersion. Extensive research has been carried out to design PhCW bends with high transmission [16,31–33], and the investigation demonstrated that dispersion was a limiting factor in

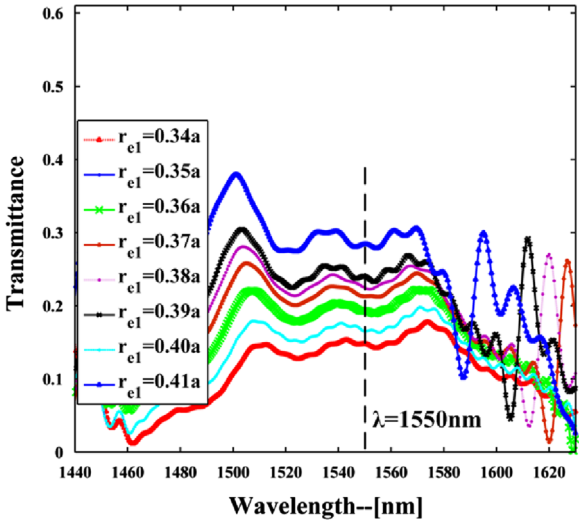

Fig. 4. The transmission spectra of 60° waveguide bend with four green holes (of radius r_{e1}) at the bend region. (For interpretation of the references to color in this figure legend, the reader is referred to the web version of this article.)

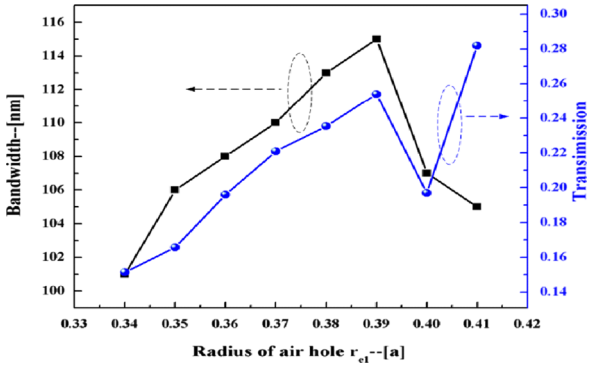

Fig. 5. 3-dB bandwidth of the bend structure and transmittance at $\lambda=1550$ nm as a function of the air hole radius r_{e1}.

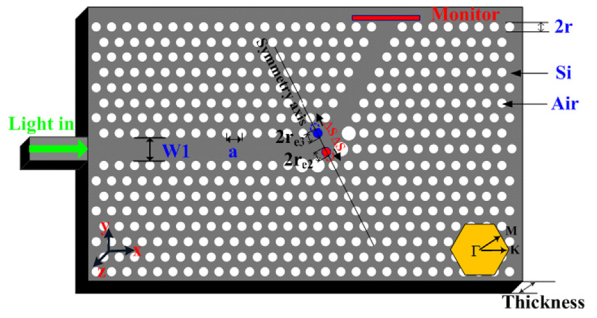

Fig. 6. Schematic view of the optimized 3D 60° bend waveguide, where $a=429$ nm, $r=0.32a$, $T=0.578$a, r_{e2} and r_{e3} are the radius of the red and blue holes at the apex of the bend, respectively; The arrows indicate the definition of the positive directions for displacement values ($\Delta\mathbf{S}$), the dashed circles indicate the position of blue and red holes after the optimization. (For interpretation of the references to color in this figure legend, the reader is referred to the web version of this article.)

Table 1
3-dB bandwidth of the bend structure and transmittance at $\lambda=1550$ nm shown in Fig. 4 versus radius of holes r_{e1}.

r_{e3}	0.34a	0.35a	0.36a	0.37a	0.38a	0.39a	0.40a	0.41a
Transmittance	0.152	0.166	0.196	0.221	0.235	0.254	0.191	0.290
Bandwidth (nm)	101	106	108	110.	13	115	107	105

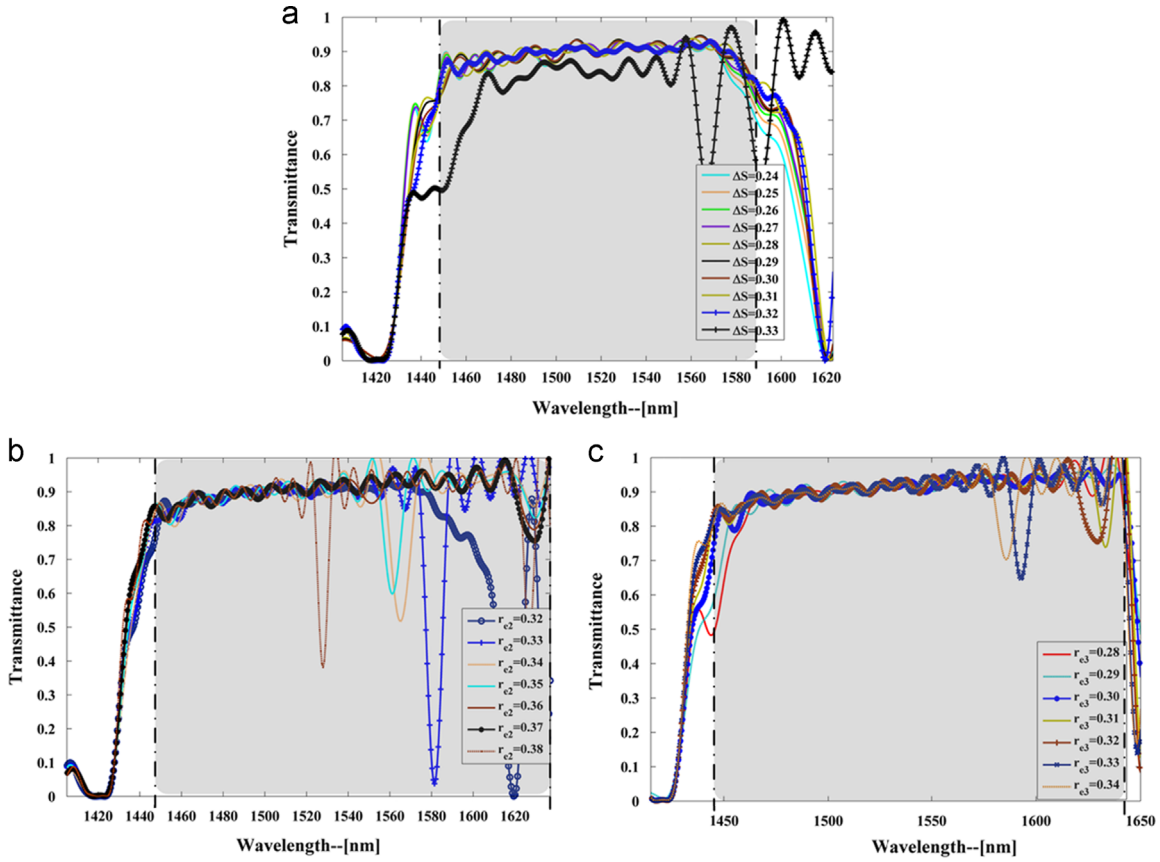

Fig. 7. (a) The transmission spectra of 60° waveguide bend as a function of the displacement $\Delta\mathbf{S}$ based on $r_{e1}=0.39a$; (b) transmittance as a function of r_{e2} based on $\Delta\mathbf{S}=0.32a$ and $r_{e1}=0.39a$; (c) transmittance as a function of r_{e3} based on $r_{e2}=0.37a$, $\Delta\mathbf{S}=0.32a$, and $r_{e1}=0.39a$. The grey region was used to discuss the flatness of transmission spectra.

Table 2a
Bandwidth, T_{max}, T_{min}, and ΔT (grey region in Fig. 7(a)) versus the displacement $\Delta\mathbf{S}$ with $r_{e1}=0.39a$. (Bandwidth is the 3-dB bandwidth of bend structure shown in Fig. 7(a)).

$\Delta\mathbf{S}$	$0.24a$	$0.25a$	$0.26a$	$0.27a$	$0.28a$	$0.29a$	$0.30a$	$0.31a$	$0.32a$	$0.33a$
Bandwidth (nm)	177	178	178	178	176	176	176	181	179	196
T_{max}	0.932	0.932	0.933	0.945	0.947	0.945	0.945	0.937	0.930	1.000
T_{min}	0.822	0.825	0.827	0.838	0.843	0.846	0.846	0.830	0.834	0.543
$\Delta T(T_{max}-T_{min})$	0.110	0.107	0.106	0.107	0.104	0.099	0.099	0.107	0.096	0.457

application of waveguides with discrete translation symmetry, which were inherently dispersive. Due to this inherently in PhC structures, any design for bends in PhCWs should consider their dispersive behavior, especially when broadband is required or in situations when an optical signal goes through a PhCW bend multiple times. A careful inspection of data presented in Table 2 based on Fig. 7 shows that the transmission spectrum of the optimized bend waveguide appears a very flat wave sharp. The high transmission (over 90%) region ranges from 1462 nm to 1643 nm, which corresponds to the expected frequency region in the band structure. Meanwhile, the 3-dB bandwidth reaches 216 nm, which is a significant improvement over other optimized bend waveguides [34–36]. Fig. 8 shows that Bandwidth and ΔT of the 60° bend waveguide as a function of $\Delta\mathbf{S}$, r_{e2}, and r_{e3}, respectively. As seen in Fig. 8, the bend waveguide obtains an optimum design structure with $\Delta\mathbf{S}=0.32a$, $r_{e2}=0.37a$, and $r_{e3}=0.30a$. Fig. 9 illustrates the calculated photonic band structure for propagation in the Γ–M direction Based on this optimized bend design. The corresponding normalized center frequency (wave vector) $a/\lambda_0=0.2408$, in this case, the wavenumbers becomes $0.1389(2\pi c/a)$, and then $k_{\Gamma M}=(3\times0.2888-0.1389)\times(2\pi/a)=0.7275(2\pi/a)$, which leads to $k_{\Gamma M}=(3\times0.2888-0.1285)\times(2\pi/a)=0.0018\times(2\pi/a)=2.936\times10^{-5}\,\mathrm{nm}^{-1}$. This is about nine times smaller than that for the conventional bend waveguide structure. It also proves that this reduced Δk (low reflection) mechanism agrees well with simulation results (high transmission).

Fig. 10 shows the steady-state magnetic field distribution for the fundamental TE-like mode of PhCWs simulated using 3D FDTD. The left image (Fig. 10(a)) presents the mode behavior for light incident from the bottom-left through the PhCW with the conventional bends. It is clearly seen that the conventional bend forms a severe discontinuity in the straight PhCW and excites an odd mode, which is not well guided in the PhCW. Furthermore, the lower bend produces large reflections of the bend region and scattering of the light to the PhC structure. On the contrary, Fig. 10(b) shows that the optimized bend regions lead the fundamental TE-like mode nicely without disturbing the mode profile. And Fig. 10(c) presents that the mode profile vertically by total internal reflection due to the refraction index differences between different layers.

To extract the bend loss the transmission spectra have been normalized to the transmission spectrum for a straight PhCW of

Table 2b
Bandwidth, T_{max}, T_{min}, and ΔT (grey region in Fig. 7(b)) versus the air hole radius r_{e2} with $\Delta\mathbf{S}=0.32a$, and $r_{e1}=0.39a$. (Bandwidth is the 3-dB bandwidth of bend structure shown in Fig. 7(b)).

r_{e2}	0.32a	0.33a	0.34a	0.35a	0.36a	0.37a	0.38a
Bandwidth (nm)	179	194	202	203	204	206	202
T_{max}	0.930	1.000	1.000	1.000	1.000	1.000	1.000
T_{min}	0.834	0.846	0.517	0.601	0.788	0.823	0.381
$\Delta T(T_{max}-T_{min})$	0.096	0.154	0.483	0.399	0.212	0.177	0.619

Table 2c
Bandwidth, T_{max}, T_{min}, and ΔT (grey region in Fig. 7(c)) versus the air hole radius r_{e3} with $r_{e2}=0.37a$, $\Delta\mathbf{S}=0.32a$, and $r_{e1}=0.39a$. (Bandwidth is the 3-dB bandwidth of bend structure shown in Fig. 7(c).)

r_{e3}	0.28a	0.29a	0.30a	0.31a	0.32a	0.33a	0.34a
Bandwidth (nm)	216	214	216	216	216	216	208
T_{max}	1.000	0.978	0.968	1.000	1.000	1.000	1.000
T_{min}	0.888	0.835	0.864	0.741	0.755	0.648	0.703
$\Delta T(T_{max}-T_{min})$	0.112	0.143	0.104	0.259	0.245	0.352	0.297

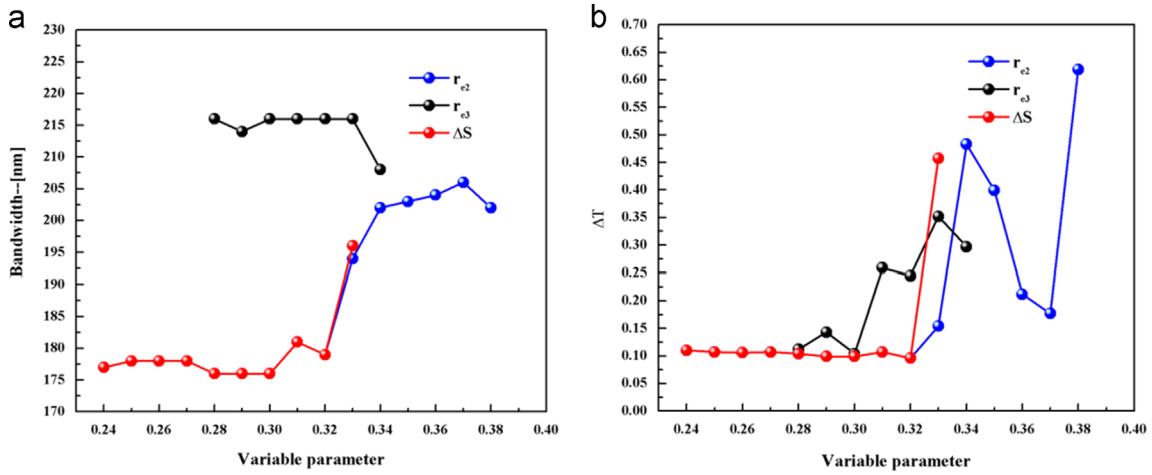

Fig. 8. (a) Bandwidth of bend waveguide as a function of $\Delta\mathbf{S}$, $r_{e2,}$ and $r_{e3;}$ (b) ΔT, based on the $r_{e1}=0.39a$.

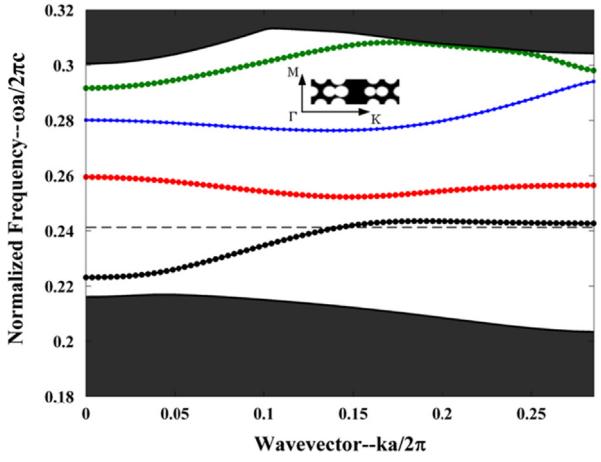

Fig. 9. Photonic band structure for the propagation along *the Γ-M* direction based on the optimum bend waveguide. The black horizontal dashed lines indicate the normalized center frequency of $a/\lambda_0=0.2408$.

the same length. Fig. 11 shows the bend loss of TE polarized light for the un-optimized generic (black curve) and the optimized (blue curve) 60° bend. In the same wavelength range the un-optimized bend clearly shows a large loss, which only reduces in a narrow range near the cut-off of the fundamental mode at longer wavelength. For the wavelength ranging from 1462 nm to 1643 nm of optimized bend covering the C-band and L-band frequency ranges, the bend loss was lower than 1 dB and an average bend loss of 0.71 ± 0.19 dB. Although waveguide bends designed by the topology optimization method [19,37] obtain less than 1 dB loss with the bandwidth more than 200 nm, many irregular shapes introduced to the bend structure bring great difficulties to device fabrication, and the physical principle of low-loss bend design is disregarded. It demonstrates that our designed 60° PhC bend waveguide can be integrated into the PICs and be applied for both C-band and L-band optical communications.

4. Conclusion

The results presented in this paper clearly show that it is possible to obtain PhCW components working for TE polarizations during the process of optimization. We also found that both mode pattern and wave number must match in order to achieve a high-transmission bend waveguide. Compared with conventional waveguide bend, this optimized design displays a 3-dB bandwidth about 216 nm and ultralow-loss (in the range 0.71 ± 0.19 dB) with the transmission above 90% output, which covers a broadband exceeding 180 nm from 1462 nm to 1643 nm. The transmission

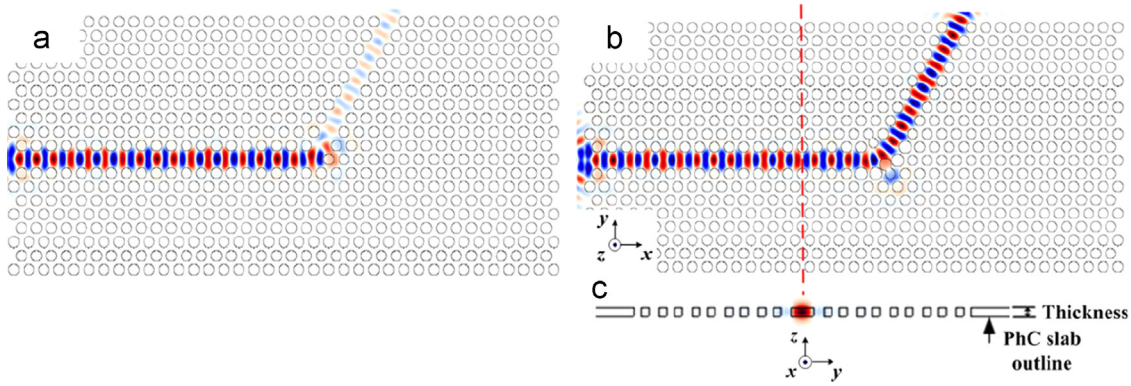

Fig. 10. Steady-state magnetic field distribution for the fundamental TE-like mode simulated using 3D FDTD. The mode is incident from the bottom-left part of the waveguide. (a) Mode profile through the conventional bend. (b) Mode profile through the optimized bend in the *x*–*y* plane. (c) Mode profile in the *y*–*z* plane.

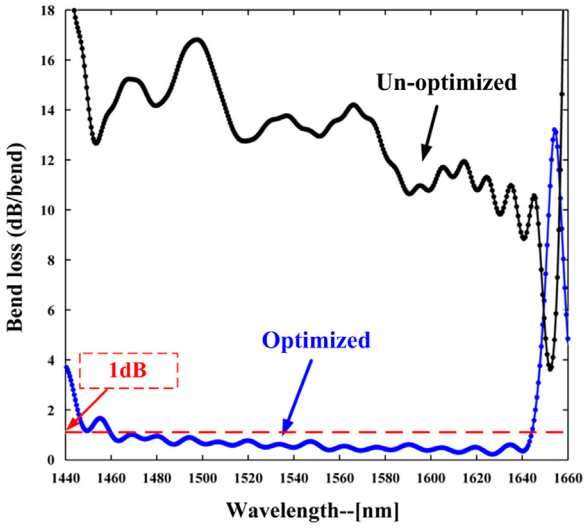

Fig. 11. Bend loss for the un-optimized 60° bend (black) and the optimized 60° bend (blue) by the 3D-FDTD simulation. Both spectra have been normalized to the transmission through straight PhCWs of the same length to eliminate the coupling and the propagation loss in straight waveguides. (For interpretation of the references to color in this figure legend, the reader is referred to the web version of this article.)

spectrum also presents flatness over 180 nm bandwidth around 1550 nm. In addition, compared with the optimization method demonstrated in Ref. [18,19], the fabrication complexity of this optimized bend waveguide is lower. Thus, this optimized design solves an important issue in actual fabrication and application and opens for the realization of a wide range of ultra-compact, low-loss, and broadband optical integrated circuit (OIC) and integrated optical devices.

Acknowledgements

This research was supported by NSFC (no. 61372038), National 973 Program (no. 2012CB315705), National 863 Program (no. 2011AA010305), Postgraduate Innovation Fund of SICE, BUPT, 2013 and Fund of State Key Laboratory of Information Photonics and Optical Communications (Beijing University of Posts and Telecommunications), PR China.

References

[1] E. Yablonovitch, Phys. Rev. Lett. 58 (1987) 2059.
[2] S. John, Phys. Rev. Lett. 58 (1987) 2486.
[3] S.G. Johnson, P.R. Villeneuve, S.H. Fan, J.D. Joannopoulos, Phys. Rev. B: Condens. Matter 62 (2000) 8212.
[4] M. Notomi, K. Yamada, A. Shinya, J. Takahashi, C. Takahashi, I. Yokohama, Phys. Rev. Lett. 87 (2001) 253902.
[5] S.H.G. Teo, A.Q. Liu, J.B. Zhang, M.H. Hong, J. Singh, M.B. Yu, N. Singh, G.Q. Lo, Opt. Express 16 (2008) 7842.
[6] S. Matsuo, K. Takeda, T. Sato, M. Notomi, A. Shinya, K. Nozaki, H. Taniyama, K. Hasebe, T. Kakitsuka, Opt. Express 20 (2012) 3773.
[7] S.W. Jeon, J.K. Han, B.S. Song, S. Noda, Opt. Express 18 (2010) 19361.
[8] C.H. Huang, W.S. Li, J.N. Wu, W.F. Hsieh, Y.C. Chang, J. Opt. Soc. Am. B: Opt. Phys. 29 (2012) 2510.
[9] J. Hou, D.S. Citrin, H. Wu, D. Gao, Z. Zhou, Opt. Lett. 36 (2011) 2263.
[10] T. Søndergaard, J. Arentoft, M. Kristensen, J. Lightwave Technol. 20 (2002) 1619.
[11] P.I. Borel, L.H. Frandsen, M. Thorhauge, A. Harpøth, Y.X. Zhuang, M. Kristensen, H.M.H. Chong, Opt. Express 11 (2003) 1757.
[12] M. Augustin, H.J. Fuchs, D. Schelle, E.B. Kley, S. NolteA. Tunnermann, Opt. Express 11 (2003) 3284.
[13] L.H. Frandsen, P.I. Borel, Y.X. Zhuang, A. Harpøth, M. Thorhauge, M. Kristensen, Opt. Lett. 29 (2003) 1623.
[14] G. Ren, W.H. Zheng, Y.J. Zhang, K. Wang, X.Y. Du, M.X. Xing, L.H. Chen, J. Lightwave Technol. 26 (2008) 2215.
[15] H. Benisty, J. Quantum Electron. 38 (2002) 770.
[16] M. Askari, B. Momeni, M. Soltani, A. Adibi, J. Lightwave Technol. 28 (2010) 1707.
[17] S. Bakhshi, Mohammad K. Moravvej-Farshi, M. Ebnali-Heidari, Appl. Opt. 50 (2011) 4048.
[18] J.H. Chen, Y.T. Huang, Y.L. Yang, M.F. Lu, J. Lightwave Technol. 30 (2012) 2345.
[19] L.H. Frandsen, A. Harpøth, P.I. Borel, M. Kristensen, J.S. Jensen, O. Sigmund, Opt. Express 12 (2004) 5916.
[20] I. Borel, A. Harpøth, L.H. Frandsen, M. Kristensen, P. Shi, J.S. Jensen, O. Sigmund, Opt. Express (2004)1996.
[21] K. Inoue, H. Oda, N. Ikeda, K. Asakawa, Opt. Express 17 (2009) 7206.
[22] J. Joannopoulos, R. Meade, J. Winn, Photonic Crystals: molding the flow of light, Princeton University Press, Princeton, 1995.
[23] A. Lavrinenko, P. Borel, L. Frandsen, M. Thorhauge, A. Harpøth, M. Kristensen, T. Niemi, H. Chong, Opt. Express 12 (2004) 234.
[24] A. Chutinan, M. Okano, S. Noda, Appl. Phys. Lett. 80 (2002) 1698.
[25] J.D. Joannopoulos, S.G. Johnson, J.N. Winn, R.D. Meade, Princeton University Press, 2008.
[26] A. Mekis, Phys. Rev. Lett. 77 (1996) 3787.
[27] C.F. Bohren, D.R. Huffman, Wiley, New York, 2008.
[28] P. Strasser, R. Wüest, F. Robin, D. Erni, H. Jäckel, J. Vac. Sci. Technol., B 25 (2007) 387.
[29] K. Rauscher, Dissertation ETH 16516, Electrical Engineering (ETH Zurich, 2006).
[30] S. Soltani, A.M. Armani, Opt. Express 21 (2013) 7748.
[31] Y. Hamachi, S. Kubo, T. Baba, Opt. Lett. 34 (2009) 1072.
[32] L. Gu, W. Jiang, X. Chen, R. Chen, IEEE Photonics Technol. Lett. 19 (2007) 342.
[33] M.-F. Lu, Y.-L. Yang, Y.-T. Huang, IEEE Photonics Technol. Lett. 20 (2008) 2114.
[34] Y. Zhang, B.J. Li, Opt. Lett. 32 (2007) 787.
[35] D. Yang, H. Tian, Y. Ji, Opt. Commun. 285 (2012) 3752.
[36] M. Zhang, N. Groothoff, A.C. Krüger, P. Shi, M. Kristensen, Opt. Express 19 (2011) 7120.
[37] A. Têtu, M. Kristensen, L.H. Frandsen, A. Harpøth, P.I. Borel, J.S. Jensen, O. Sigmund, Opt. Express 13 (2005) 8606.